Rotationally resolved photoelectron spectroscopy of hot N 2 formed in the photofragmentation of N 2 O

Anouk M. Rijs, Ellen H. G. Backus, Cornelis A. de Lange, Maurice H. M. Janssen, Kwanghsi Wang, and Vincent McKoy

Citation: The Journal of Chemical Physics **114**, 9413 (2001); doi: 10.1063/1.1370078
View online: http://dx.doi.org/10.1063/1.1370078
View Table of Contents: http://scitation.aip.org/content/aip/journal/jcp/114/21?ver=pdfcov
Published by the AIP Publishing

Rotationally resolved photoelectron spectroscopy of hot N_2 formed in the photofragmentation of N_2O

Anouk M. Rijs
Laboratory of Physical Chemistry, University of Amsterdam, Nieuwe Achtergracht 127-129, 1018 WS, Amsterdam and Laser Center and Department of Chemistry, Vrije Universiteit, De Boelelaan 1083, 1081 HV Amsterdam, The Netherlands

Ellen H. G. Backus and Cornelis A. de Lange[a)]
Laboratory of Physical Chemistry, University of Amsterdam, Nieuwe Achtergracht 127-129, 1018 WS, Amsterdam, The Netherlands

Maurice H. M. Janssen
Laser Center and Department of Chemistry, Vrije Universiteit, De Boelelaan 1083, 1081 HV Amsterdam, The Netherlands

Kwanghsi Wang and Vincent McKoy
Arthur Amos Noyes Laboratory for Chemical Physics, California Institute of Technology, Pasadena, California 91125

(Received 13 February 2001; accepted 14 March 2001)

The photoionization dynamics of rotationally hot molecular nitrogen are studied employing resonance enhanced multiphoton ionization in combination with photoelectron spectroscopy. Photodissociation of N_2O at ~203 nm results in highly rotationally excited N_2 fragments in $X\,^1\Sigma_g^+(N'',v''=0,1)$ states and O atoms in the excited $^1D_2$ state. Photoelectron detection of the rotationally hot N_2 states is performed by a two-photon excitation to the lowest $a''\,^1\Sigma_g^+$ Rydberg state followed by one-photon ionization. The large number of observed rotational levels, from $N'=49$ up to $N'=94$, results in improved rotational parameters for $a''\,^1\Sigma_g^+$ $(v'=0)$. In addition, experimental and theoretical rotationally resolved photoelectron spectra of the $a''\,^1\Sigma_g^+(v'=0,1;N')$ state are presented. In these spectra only $\Delta N=N^+-N'=$*even* transitions are observed, with a dominant $\Delta N=0$ peak and rather weak $\Delta N=\pm 2$ peaks. The one-photon ionization is dominated by ejection of electrons in *p* and *f* partial waves. The agreement between experimental and calculated spectra is excellent. © *2001 American Institute of Physics.*
[DOI: 10.1063/1.1370078]

I. INTRODUCTION

Nitrous oxide (N_2O) plays an important role in the chemistry of the earth's atmosphere. In the lower atmosphere, nitrous oxide is a prominent greenhouse gas, and in the stratosphere it contributes to the catalytic depletion of ozone.[1,2] the photolysis of atmospheric N_2O by absorption of solar radiation in the 200 nm range forms oxygen atoms in the excited $^1D_2$ state, and N_2 in its electronic ground state.[3] The production of these very reactive oxygen atoms is an important reason why even relatively small quantities of N_2O are still atmospherically relevant. In the stratosphere N_2O can subsequently undergo extensive oxidation reactions with excited $O(^1D)$, to produce N_2 and O_2, as well as NO, and higher nitrogen oxides. In fact, photo-oxidation reactions are an important source of the formation of stratospheric nitrogen oxides (NO_x), which are now known to be crucial in the ozone cycle. They play an important role in catalytic ozone destruction processes.

The molecule N_2O is linear ($C_{\infty v}$) in its electronic ground state. Upon absorption of one or more photons, the molecule may undergo a transition to a bent configuration with C_s symmetry. Excited electronic states, thought to play a role in the photofragmentation of N_2O around 200 nm, are $\tilde{A}\,^1\Sigma^-$ and $\tilde{B}\,^1\Delta$ (in $C_{\infty v}$ symmetry), correlating to $1\,^1A''$ and $2\,^1A'$, $2\,^1A''$, respectively (in C_s symmetry).[4] The photodissociation of N_2O in the spectral region near 200 nm occurs mainly *via* the one-photon forbidden repulsive $\tilde{B}\,^1\Delta$ $(2\,^1A')$ state, leading to N_2 $(X\,^1\Sigma_g^+)$ and O $(^1D_2)$.[5,6] The $2\,^1A'$ state is highly anisotropic and has a minimum energy in the Franck–Condon region at a bending angle of about 130°.[5] As the fragments separate, a strong torque will be exerted on the N_2 photofragments, resulting in rotationally ''hot'' N_2. Several experimental techniques, including resonance-enhanced multiphoton ionization (REMPI), either in conjunction with mass-resolved ion detection,[7] or ion imaging,[5,8–12] have been used to probe the product channels. All these studies of the photodissociation of N_2O have focused on elucidating the details of the various photodissociation pathways, and on measuring the energy and angular distributions of N_2.

REMPI of N_2 is not a trivial matter, and relatively few excited states have so far been utilized as stepping stones in an $(n+m)$ REMPI process. The reasons for this are the high ionization energy of ~15.6 eV, the large energy separation between the electronic ground state and most excited states,

a)Electronic mail: deLange@fys.chem.uva.nl

and the strict optical selection rules which arise from the symmetry restrictions associated with this homonuclear diatomic molecule. The lowest Rydberg state $a''\,^1\Sigma_g^+$, located about ~12 eV above the electronic ground state, and accessed by a two-photon ($\lambda \sim 203$ nm) allowed excitation of an electron in the highest occupied $3\sigma_g$ orbital to the $4\sigma_g(n=3)$ Rydberg orbital, was used for the first time in a (2+1) REMPI study[13] as a convenient stepping stone. The $a''\,^1\Sigma_g^+$ state represents the lowest member of a Rydberg series converging upon the $X\,^2\Sigma_g^+$ ionic ground state of N_2^+. In this work the dominant *Q* branch was used in the intermediate excitation $a''\,^1\Sigma_g^+ \leftarrow\leftarrow X\,^1\Sigma_g^+$ to study the subsequent photoionization process. From the *Q*-branch photoexcitation information on the relative vibrational and rotational populations of the electronic ground state can be obtained directly. In a similar study high-resolution (2+1) REMPI spectroscopy was performed on the (0,0), (1,1), and (2,2) transitions of the $a''\,^1\Sigma_g^+ \leftarrow\leftarrow X\,^1\Sigma_g^+$ two-photon absorption in N_2.[14,15] In addition, accurate vibrational and rotational constants of the excited $a''\,^1\Sigma_g^+$ Rydberg state were obtained based on rotational levels up to $J'=39$.[14]

The experimental vibrational and rotational energy distributions of N_2, generated in the photofragmentation of N_2O, have been studied by also employing (2+1) REMPI *via* the $a''\,^1\Sigma_g^+(\nu') \leftarrow\leftarrow X\,^1\Sigma_g^+(\nu'')$ transitions.[7] The *Q* branches were again found to dominate strongly over *O* and *S* branches. It was concluded that the N_2 fragments are predominantly formed in their electronic and vibrational ground state, but with high rotational energies. The rotational energy distribution peaks with a single maximum at rotational level $J''=74$. Several peaks above $J''=77$ were also observed, but remained unassigned. The authors suggested that these peaks might be due to perturbations in the $N_2 a''\,^1\Sigma_g^+$ state.[7]

In recent ion imaging experiments of the photodissociation of N_2O at Sandia Livermore and VU Amsterdam[5,9–11] state-specific angular and velocity distributions for the individual rovibrational levels of the N_2 photofragment and O (^1D) atom were obtained. In these studies rotationally ''hot'' N_2 fragments were observed, again with a rotational distribution peaking at $J''=74$. Furthermore, initial assignments of the $a''\,^1\Sigma_g^+ \leftarrow\leftarrow X\,^1\Sigma_g^+$ transitions above $J'=77$ ($\nu'=0$), which were previously ascribed to perturbations in the $a''\,^1\Sigma_g^+$ intermediate state,[7] revealed the production of N_2 in its first excited vibrational state ($\nu''=1$). By combining the O (^1D) and N_2 measurements, velocity-resolved determinations of the O (^1D) orbital alignment and angular distributions were obtained. An analysis of the observed dynamical effects was carried out,[5,9,11] based on the results of theoretical calculations of the potential energy surfaces of N_2O.[4,16] These results were employed to estimate the branching ratio between the two bent excited states. For the highest J' levels (above $J'=74$), corresponding to the highest degree of bending of the parent N_2O, the photodissociation occurs almost completely *via* the $2\,^1A'$ ($\tilde{B}\,^1\Delta$) state.[5]

REMPI in combination with mass-resolved ion detection has the disadvantage that no experimental information can be obtained about the final state of the ion. Albeit experimentally more demanding, REMPI in conjunction with kinetic-energy-resolved electron detection, also termed laser photoelectron spectroscopy (PES), possesses unique capabilities. The rules of energy and momentum conservation allow the experimentalist to determine the internal energies of the ions formed in the two-step photoabsorption process. The determination of ion internal energies (electronic, vibrational, and rotational) is a true asset of the method, and laser photoelectron spectroscopy offers very significant advantages, which are not easily matched in its broad applicability by other techniques.[17–19]

When the resolution of the electron spectrometer used is sufficient, ion rotational levels can be resolved, and ion rotational branching ratios can be measured. From angular momentum considerations very detailed information about the photoionization dynamics of simple molecules can be obtained, especially if these experiments can be compared with the results of high-level *ab initio* theoretical calculations.[20,21] With the REMPI method, a single rotational level of the resonant intermediate state is selected, so that only a few rotational levels of the ion are accessed. Rotational resolution in the ion is easily achieved, if the rotational constants of the ionic state under consideration lead to ionic rotational spacings large compared to the spectrometer resolution. This is usually the case for diatomic hydrides, and a plethora of rotationally resolved PE studies have been performed on such light molecules. Representative cases are stable molecules such as diatomic hydrogen[22–25] and its isotopomer D_2,[26,27] and several short-lived diatomic hydride radicals such as OH,[28] NH,[29,30] and SH.[31,32]

The present paper is concerned with rotationally resolved laser photoelectron spectroscopy of hot N_2 photofragments using the $a''\,^1\Sigma_g^+$ intermediate state. The rotational constant of N_2^+ in the $X\,^2\Sigma_g^+$ ionic ground state is only 1.922 321 cm^{-1}.[33] However, the high rotational excitation of the N_2 fragments following photodissociation of the N_2O parent accesses ionic rotational levels with high J^+, and hence leads to a situation where the ionic rotational spacings exceed the spectrometer resolution. The results of our experiments are compared to those of advanced *ab initio* quantum-chemical calculations, a strategy that has proved its worth in many cases,[28,30,31] and which gives detailed information about the dynamics of the photoionization process. In addition, improved values of rovibrational parameters of the $a''\,^1\Sigma_g^+$ Rydberg state are obtained.

In Sec. II a brief description of the experimental setup is given and in Sec. III a brief outline of the theoretical formulation is given. The measured and calculated spectra are presented and discussed in Sec. IV. The conclusions are summarized in Sec. V.

II. EXPERIMENT

A description of the laser system and the ''magnetic bottle'' spectrometer has been reported in great detail recently.[34] Therefore, the experimental setup is described only briefly here.

The laser system consists of a XeCl excimer laser (Lumonics HyperEx 460), operating at a 30 Hz repetition rate, which pumps a Lumonics HyperDye 500 dye laser (bandwidth 0.08 cm^{-1}), operating on Rhodamine B. The dye laser

output (around 610 nm) is frequency doubled using a Lumonics HyperTrack 1000, with an angle-tuned *KD*P* crystal. A zero-order half-lambda waveplate (CVI) is used to rotate the polarization of the fundamental laser beam by 90°, while maintaining the polarization of the frequency-doubled beam. The rotated fundamental and the frequency-doubled laser beams are sum-frequency mixed in an angle-tuned BBO crystal to generate ultraviolet light around 203 nm. The fundamental and the harmonic beams are spatially separated by a Pellin–Broca prism to yield a vertically polarized 203 nm beam. The typical pulse energy used in these experiments is 0.1 μJ. During the wavelength scans the power of the 203 nm laser beam is monitored with a photodiode. The laser light is focused into the ionization region of the ''magnetic bottle'' spectrometer by a quartz lens with a focal length of 25 mm. In the present experiments the ''magnetic bottle'' spectrometer is used exclusively in the electron detection mode, with a collection efficiency of ~50%.

The rotationally hot N_2 photofragments are generated *in situ* by one-photon dissociation of neat N_2O (Matheson). The N_2O gas is effusively introduced into the ''magnetic bottle'' spectrometer. The photodissociation of N_2O as well as the subsequent (2+1) REMPI of the ''hot'' N_2 fragments, is performed with the same laser photons of 203 nm.

Two kinds of experiments are performed. First, the resonant excited states are located by scanning the excitation wavelength and monitoring the electron current of N_2, selecting a small kinetic-energy window of photoelectrons. Second, for several resonances photoelectron spectra are measured at a fixed excitation wavelength. For calibration of both the wavelength and the photoelectron kinetic energies, well-known resonances of krypton atoms in combination with the oxygen atom resonances were used.

III. THEORY AND NUMERICAL DETAILS

The general theory of molecular REMPI processes used in the present study has been described previously.[35] Here we present just a brief outline of some essential features as it is used to obtain rotationally resolved photoelectron spectra. In the present case, ionization originating from each of the $(2J+1)$ magnetic sublevels of the $a''\,^1\Sigma_g^+$ state of N_2 forms an independent channel. The total cross section σ for ionization of a J level of the intermediate state leading to a J^+ level of the ion can be written as

$$\sigma \propto \sum_{\substack{lm \\ M_J, M_{J^+}}} \rho_{M_J M_J} |C_{lm}(M_J, M_{J^+})|^2, \tag{1}$$

where $\rho_{M_J M_J}$ is the population of a specific M_J level of the intermediate state. The coefficients $C_{lm}(M_J, M_{J^+})$ of Eq. (1) are related to the probability for photoionization of the M_J level of the intermediate state leading to the M_{J+} level of the ionic state. The $C_{lm}(M_J, M_{J^+})$ coefficients, which explicitly consider the spin coupling associated with multiplet-specific final state wave functions and a Hund's case (b) coupling scheme, have the form

$$\begin{aligned} C_{lm}(M_J, M_{J^+}) = & \sqrt{\frac{4\pi}{3}}[(2N^+ + 1)(2N+1)(2J+1)(2J^+ + 1)(2S+1)]^{1/2} \\ & \times \sum (-1)^P (2N_t + 1) \begin{pmatrix} N & S & J \\ M & M_S & -M_J \end{pmatrix} \begin{pmatrix} N^+ & S^+ & J^+ \\ M^+ & M_{S^+} & -M_{J^+} \end{pmatrix} \begin{pmatrix} S^+ & 1/2 & S \\ M_{S^+} & M_\sigma & -M_S \end{pmatrix} \begin{pmatrix} N^+ & N & N_t \\ -M^+ & M & m_t \end{pmatrix} \\ & \times \begin{pmatrix} N_t & 1 & l \\ -m_t & \mu_0 & -m \end{pmatrix} \sum_{\substack{\mu \\ \lambda_t}} (-1)^{-\Lambda^+ - \mu} \tilde{I}_{l\lambda\mu} \begin{pmatrix} N^+ & N & N_t \\ -\Lambda^+ & \Lambda & \lambda_t \end{pmatrix} \begin{pmatrix} N_t & 1 & l \\ -\lambda_t & \mu & -\lambda \end{pmatrix}, \end{aligned} \tag{2}$$

with

$$P = M^+ + M_{J^+} - M + \mu_0 - N - N^+ + s + \tfrac{1}{2}, \tag{3}$$

$$\tilde{I}_{l\lambda\mu} = (-i)^l e^{i\eta_l} \int dR\, \chi^*_{v^+}(R) r^{l\lambda\mu}_{fi}(R) \chi_{v_i}(R), \tag{4}$$

$$\begin{aligned} r^{l\lambda\mu}_{fi}(R) = & \sum_{l', l_0} \langle g_{l,l'\lambda}(k,r,R) Y_{l'\lambda}(\hat{r}') | r Y_{1\mu} | \\ & \times \phi_{il_0}(r,R) Y_{l_0,\lambda_0}(\hat{r}') \rangle, \end{aligned} \tag{5}$$

where λ and m are projections of the photoelectron's angular momentum l in the molecular and laboratory frames, respectively, Λ is the projection of electronic orbital angular momentum along the internuclear axis, S is the total spin, R denotes a dependence on internuclear distance, $\tilde{I}_{l\lambda\mu}$ is the vibrationally averaged photoelectron matrix element between the resonant state and the photoelectron continuum wave function, and μ and μ_0 are the light polarization index in the molecular and laboratory frame, respectively. The symbols with superscript + are related to the same quantities in the ion. In Eq. (5), we have employed single-center expansions of a partial wave component of the photoelectron orbital, $\psi^{(-)}_{klm}(\mathbf{r})$ and of the initial orbital $\phi_i(\mathbf{r}')$, where ionization originates, i.e.,

$$\psi^{(-)}_{klm} = \sum_{l'\lambda} g_{l,l'\lambda}(k,r) D^l_{m\lambda} Y_{l\lambda}(\hat{r}), \tag{6}$$

with

$$\Psi^{(-)}_{f,\mathbf{k}} = \left(\frac{2}{\pi}\right)^{1/2} \sum_{lm} i^l \psi^{(-)}_{klm}(\mathbf{r}) Y^*_{lm}(\mathbf{k}), \tag{7}$$

TABLE I. Comparison of rotational constants (cm^{-1}) of the lowest excited Rydberg state $a''\,^1\Sigma_g^+(v'=0)$ of N_2 from this work and from the literature (see Ref. 12).

Constants	Present work (cm^{-1})	Ref. values[a] (cm^{-1})
v_{00}	98 840.41(9)	98 840.59(0.12)
B_0'	1.91439(4)	1.9143(2)
$D_0'\times 10^6$	6.143(2)	6.6(2)

[a]See Ref. 13.

where $\Psi_{f,\mathbf{k}}^{(-)}$ is the photoelectron continuum orbital. Equation (2) yields the selection rule

$$\Delta N + l = odd, \tag{8}$$

for photoionization of these Σ–Σ transitions. Since the $4\sigma_g$ orbital contains mainly *s* character, (94.22% *s*, and 5.58% *d*), the *p* wave component of the photoelectron matrix element should be dominant (there are no even partial waves), so only even ΔN transitions are expected.

For the wave function of the $a''\,^1\Sigma_g^+$ resonant state, we use the improved virtual orbital method[36] in which the core orbitals are taken to be those of the fully relaxed $^2\Sigma_g^+$ ion and the $4\sigma_g$ resonant orbital is obtained as an eigenfunction of the static-exchange potential of the core. The orbital basis used in these calculations consists of a [4,3] contraction of the (9,5) primitive Gaussian basis[37] augmented by one *s* function ($\alpha=0.08$), one *p* function ($\alpha=0.075$), and two *d* functions ($\alpha=1.4836$, and 0.4691) on the nitrogen atom. At the molecular center, we add three *s* functions ($\alpha=0.06$, 0.02, and 0.008), three *p* functions ($\alpha=0.035$, 0.012, and 0.005), and two *d* functions ($a=0.12$ and 0.025). With this basis and choice of wave functions, we obtain a self-consistent-field energy of $-108.532\,032\,9$ a.u. at $R=2.12$ a.u. for the $a''\,^1\Sigma_g^+$ state. In this basis set, the ground state Hartree–Fock energy is $-108.976\,61$ a.u. at the experimental equilibrium geometry of $R=2.068$ a.u. The energy difference between the calculated ground and excited state energies is 12.09 eV. This is in good agreement with the experimental $v=0$ band origin of 12.25 eV (see also Table I).

For the final state we assume a frozen-core Hartree–Fock model in which the core orbitals are taken to be those of the $^2\Sigma_g^+$ ion and the photoelectron orbital is a solution of the one-electron Schrödinger equation. We obtain the photoelectron orbitals used in these calculations numerically employing an iterative procedure to solve the Lippmann–Schwinger equation associated with the one-electron Schrödinger equation. The radial grid used in the numerical integration of these equations extended out to 64 a.u. and contained 800 points.

IV. RESULTS AND DISCUSSION

Since all the experiments are carried out with one laser only, the photodissociation wavelength is not constant. Therefore, both the internal state distribution and the total yield of N_2 may vary as the wavelength is scanned. N_2O is known to possess an absorption spectrum extending from 220 to 170 nm.[38] The cross section shows distinct structure superimposed on top of a smooth continuum, especially in the region around the peak of the absorption band ~182 nm. Around 203 nm the spectrum is not showing any structure at room temperature. We expect that under these conditions, over the 1.5 nm range studied, the photodynamics of N_2O in the effusive beam will not be strongly influenced.

The molecular ground and excited states involved in our experiments, as well as the lowest ionic state, all have Σ symmetry. Therefore, these states can be conveniently treated in a Hund's case (b) coupling [Eq. (2)], in which we only focus on the end-over-end rotation N'', N', and N^+. Rotational structure in the photoelectron spectra of a homonuclear diatom, ionized in a (2+1) multiphoton absorption process, is subject to rotational selection rules [Eq. (8)].[39] Selection rules predict that for one-photon ionization from the $a''\,^1\Sigma_g^+(v';N')$ levels, only $\Delta N+l=odd$ transitions are allowed, where $\Delta N=N^+-N'$, and l is a partial wave component of the photoelectron. In an atomic-like picture, removal of the $4\sigma_g(n=3)$ Rydberg electron is expected to lead to *p* ($l=1$) partial waves and, hence, only $\Delta N=even$ transitions would be expected in the photoelectron spectra. Moreover, additional selection rules for homonuclear diatomics, based on inversion symmetry, also predict odd partial waves for the one-photon ionization from the $a''\,^1\Sigma_g^+$ to the $X\,^2\Sigma_g^+$ ionic state.[39]

Conservation of angular momentum also requires $\Delta N = l+1, l, \ldots, -l-1$, where l is an angular momentum component of the photoelectron. Combined with selection rules [Eq. (8)], the allowed transitions for a *p* wave are limited to $\Delta N=0,\pm 2$, while for an electron leaving in an *f* wave $\Delta N=0,\pm 2,\pm 4$ holds. All our observations agree with these predictions.

In the assignments of our photoelectron spectra, the boson nuclear spin statistics of $^{14}N\,^{14}N$, the most abundant isotopomer of N_2, must also be considered. In the $a''\,^1\Sigma_g^+$ excited states of molecular nitrogen, even values of N' can only exist in conjunction with nuclear spin wave functions which are symmetrical under permutation of the spins. Conversely, odd values of N' can only exist in combination with nuclear spin functions which are antisymmetrical under permutation. The ratio of symmetrical to antisymmetrical nuclear spin functions is 2:1. In the $X\,^2\Sigma_g^+$ ionic ground state of molecular nitrogen, even N^+ levels exist in combination with symmetrical, odd N^+ levels with antisymmetrical nuclear spin functions. Therefore, in our experiments either even or odd N^+ levels are expected to be accessed in the ionic state.

At 203 nm, the photodissociation of N_2O produces rotationally hot N_2 photofragments, mostly in its vibrational ground state.[6,7] Figure 1 shows a two-photon excitation spectrum of the N_2 photofragments in the two-photon energy range 98 100–98 700 cm^{-1}. The spectrum was obtained by monitoring photoelectrons with a kinetic energy of about 2.8 eV. These photoelectrons arise from the (2+1) photoionization process, starting from the $X\,^1\Sigma_g^+$ $(v''=0,1;J'')$ ground state to the $X\,^2\Sigma_g^+(v^+=0,1;N^+)$ lowest ionic state, *via* the $a''\,^1\Sigma_g^+(v'=0,1;N')$ intermediate Rydberg state. All the observed transitions are of *Q* type ($\Delta N=0$). The rotationally-

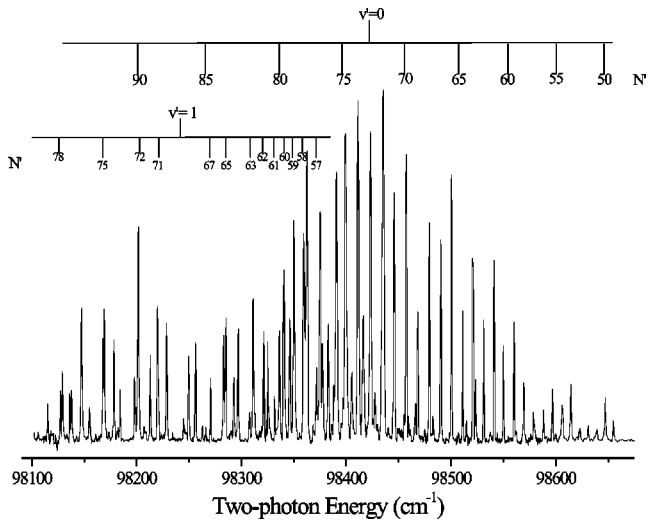

FIG. 1. Two-photon excitation spectrum of the Q branch of the $a''\,^1\Sigma_g^+ \leftarrow\leftarrow X\,^1\Sigma_g^+$ transition of hot N_2 photofragments in the two-photon energy range 98 100–98 800 cm^{-1} (vacuum energies), obtained by monitoring photoelectrons with a kinetic energy of approximately 2.8 eV.

resolved wavelength spectrum reflects the rotational distribution of N_2 in the $a''\,^1\Sigma_g^+$ state, extending from $N'=49$ up to $N'=94$. At low N' ($N'=49-77$) an even/odd intensity alternation is observed, with transitions originating from even N' more intense due to nuclear spin statistics. The comb above the spectrum in Fig. 1 presents the assignment of the N' rotational levels of the Q-branch transitions arising from $X\,^1\Sigma_g^+(v''=0,1;N'')$.

Our excitation spectrum is in good agreement with the spectrum recorded by Hanisco and Kummel,[7] by Neyer *et al.*,[9] and by Teule.[11] Our spectrum is measured with an effusive beam of pure N_2O, while the other groups employed pulsed molecular beams. Hanisco and Kummel[7] used a molecular beam of He with 35% N_2O, Neyer *et al.*[9] a pure beam, and Teule[11] a hexapole state-selected seeded beam. This indicates that the use of an effusive beam has a negligible effect on the N_2 distribution at low N' levels ($N'<77$). However, below 98 375 cm^{-1} our spectrum shows much more structure.

Towards the red end of the spectrum (below 98 375 cm^{-1}) some irregularities in the spectrum arising from N_2 $X\,^1\Sigma_g^+$ ($v''=0$) appear. Hanisco and Kummel[7] were not able to assign these multiple peaks, and suggested that they might be due to local perturbations in the N_2 $a''\,^1\Sigma_g^+$ state. Neyer *et al.*,[9] using an ion-imaging technique, assigned these peaks in part as a superimposed structure of rotational states arising from $X\,^1\Sigma_g^+$ ($v''=0$) and overlapping transitions from $X\,^1\Sigma_g^+(v''=1;N'')$. By using REMPI in combination with kinetic-energy-resolved electron detection, we were able to obtain a much more structured and resolved excitation spectrum, especially at the red end of the spectrum. Therefore, we have been able to assign the perturbed peaks of N_2 ($v'=0$), $N'>77$ up to $N'=94$. We also assigned the overlapping transitions of N_2 in the first vibrationally excited state (1,1 transition).

The assignment of the peaks in Fig. 1 and the rotational analysis were carried out using the published line positions

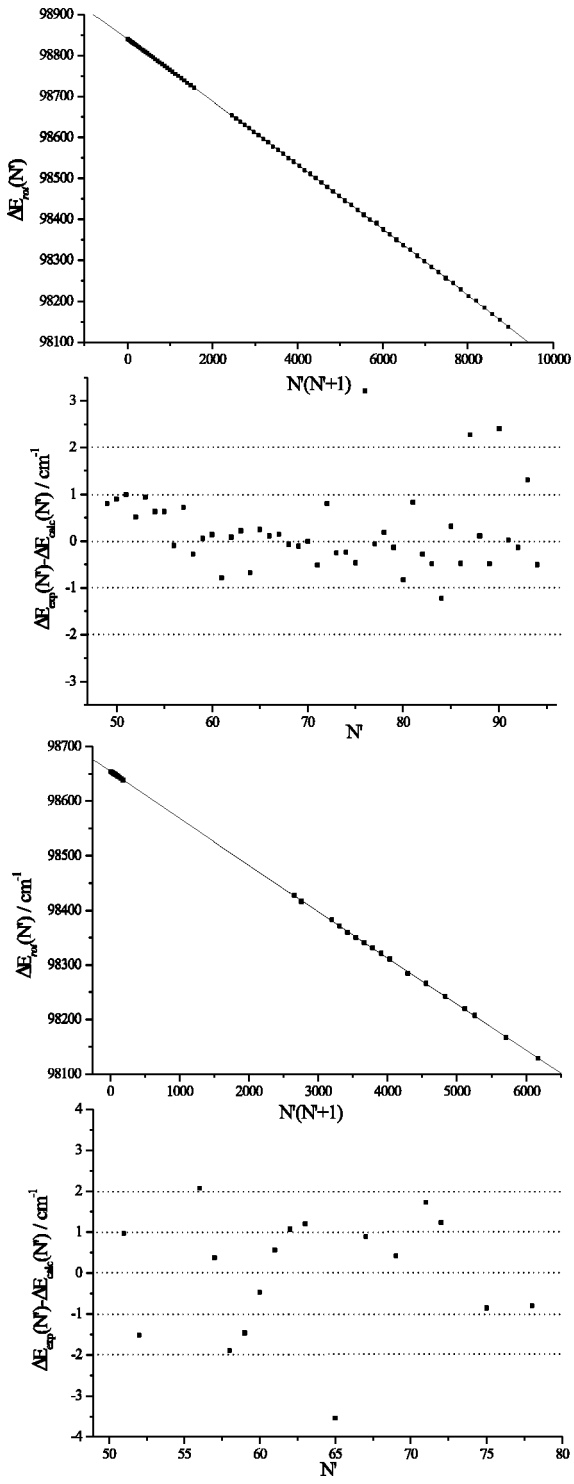

FIG. 2. (a) Fit of observed rotational level energies for the $a''\,^1\Sigma_g^+(v'=0)$ Rydberg state, based on the rotational constants of the vibrationless ground state $X\,^1\Sigma_g^+(v''=0)$ of N_2 (Ref. 18), and on the improved constants for the $a''\,^1\Sigma_g^+(v'=0)$ state given in Table I. (b) Difference between experimental and calculated line positions for the $a''\,^1\Sigma_g^+$ ($v'=0$) Rydberg state; (c) similar to (a) but for the $a''\,^1\Sigma_g^+(v'=1)$ Rydberg state; (d) similar to (b) but for the $a''\,^1\Sigma_g^+(v'=1)$ Rydberg state.

(low N' values) of Hanisco and Kummel,[14] by assigning the measured rotational lines in an iterative fashion. By using the published ground state rotational constants,[40] the excited state rotational constants were determined by fitting all the

TABLE II. Line positions (cm^{-1}) of the rotational levels of the $a''\,^1\Sigma_g^+(v'=0) \leftarrow\leftarrow X\,^1\Sigma_g^+(v''=0)$ Q-branch transitions. The left column shows the measured line positions, the middle column the calculated line positions, obtained with the improved rotational constants given in Table I. The right column shows the differences between experimental and calculated line positions.

	(0,0) transition		(1,1) transition	
N'	Measured $Q(N')$	Fit $Q(N')$	Measured $Q(N')$	Fit $Q(N')$
49	98 654.73	98 653.92	⋯	⋯
50	98 647.11	98 646.21	⋯	⋯
51	98 639.34	98 638.34	98 427.96	98 426.83
52	98 630.82	98 630.30	98 416.59	98 417.94
53	98 623.05	98 622.11	⋯	98 408.89
54	98 614.38	98 613.75	⋯	98 399.68
55	98 605.86	98 605.22	⋯	98 390.30
56	98 596.44	98 596.53	98 382.99	98 380.75
57	98 588.4	98 587.68	98 371.59	98 371.04
58	98 578.38	98 578.66	98 359.44	98 361.17
59	98 569.53	98 569.47	98 349.84	98 351.13
60	98 560.26	98 560.12	98 340.63	98 340.93
61	98 549.82	98 550.6	98 331.3	98 330.56
62	98 541.00	98 540.91	98 321.28	98 320.04
63	98 531.28	98 531.06	98 308.08	98 309.35
64	98 520.36	98 521.03	⋯	98 298.50
65	98 511.09	98 510.84	98 285.34	98 287.48
66	98 500.59	98 500.47	⋯	98 276.31
67	98 490.09	98 489.94	98 266.06	98 264.97
68	98 479.17	98 479.23	⋯	98 253.47
69	98 468.25	98 468.36	98 242.38	98 241.82
70	98 457.30	98 457.30	⋯	98 230.00
71	98 445.57	98 446.08	98 219.88	98 218.02
72	98 435.49	98 434.68	98 207.25	98 205.89
73	98 422.86	98 423.11	⋯	98 193.59
74	98 411.13	98 411.36	⋯	98 181.14
75	98 398.98	98 399.44	98 167.77	98 168.53
76	98 390.55	98 387.34	⋯	98 155.76
77	98 375.01	98 375.06	⋯	98 142.84
78	98 362.8	98 362.61	98 129.01	98 129.76
79	98 349.84	98 349.97	⋯	⋯
80	98 336.34	98 337.16	⋯	⋯
81	98 325.00	98 324.17	⋯	⋯
82	98 310.72	98 310.99	⋯	⋯
83	98 297.16	98 297.64	⋯	⋯
84	98 282.88	98 284.1	⋯	⋯
85	98 270.70	98 270.38	⋯	⋯
86	98 256.00	98 256.47	⋯	⋯
87	98 244.66	98 242.38	⋯	⋯
88	98 228.22	98 228.11	⋯	⋯
89	98 213.16	98 213.64	⋯	⋯
90	98 197.98	98 199.00	⋯	⋯
91	98 184.18	98 184.16	⋯	⋯
92	98 169.00	98 169.13	⋯	⋯
93	98 155.23	98 153.92	⋯	⋯
94	98 138.01	98 138.51	⋯	⋯

rotational energies of the Q-branch transitions to the following expression:

$$\Delta E(N') = v_{v'v''} + (B_v' - B_v'')N'(N'+1) - (D_v' - D_v'')N'^2(N'+1)^2. \quad (9)$$

The results of a least-squares-fitting procedure, including our new high N' transitions, are shown in Fig. 2(a) (0–0) transition) and 2(c) (1–1 transition). The improved rotational constants for $a''\,^1\Sigma_g^+(v'=0)$ are listed in Table I. Addition of the third order constant (H_v') did not provide a significant improvement of the rotational fit. The measured and calculated line positions are listed in Table II. The differences between experimental and calculated line positions are presented in Fig. 2(b) (0,0 transition) and 2(d) (1,1 transition). A local perturbation at $N'=76(v'=0)$ can be clearly seen in the difference plot in Fig. 2(b). Also, perturbations at $N'=87,90,93(v'=0)$ can be observed. They may be caused by the interfering vibrationally excited (1,1) Q-branch transitions. These line positions were left out in the least-squares-fitting procedure. Also, somewhat larger deviations are observed in the difference plot [Fig. 2(d)] of the (1,1) Q branch.

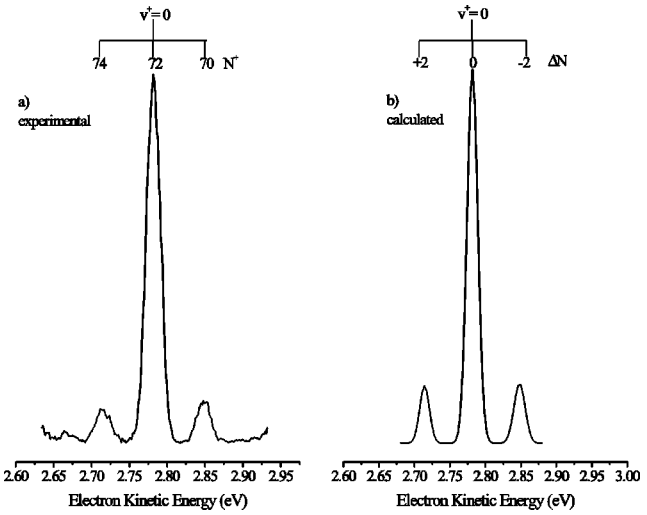

FIG. 3. Measured (left) and calculated (right) rotationally resolved photoelectron spectra of rotationally excited N_2, generated in the photofragmentation of N_2O. The spectra are obtained by (2+1) photoionization *via* the $Q(72)$ transition of the intermediate $a''\,^1\Sigma_g^+(v'=0)$ state.

Figure 3 presents the measured [Fig. 3(a)] and calculated [Fig. 3(b)] photoelectron spectra obtained for (2+1) photoionization *via* the (0,0) $Q(72)$ rotational transition at 98 435.49 cm^{-1}, leading to the $X\,^2\Sigma_g^+(v^+=0,N^+)$ ionic ground state of N_2^+. The dominant peak in the photoelectron spectrum at about 2.78 eV is the $\Delta N=0$ transition of the Q branch. The neighboring peaks arise from $\Delta N=\pm 2$ transitions. No photoelectron peaks are observed for $\Delta N=\pm 1$ transitions due to the selection rules for N_2.[34] The rotational spacings between the $\Delta N=0$ and $\Delta N=+2$ and -2 peaks are $B^+(4N^++6)$(70 meV) and $B^+(4N^+-2)$(68 meV), respectively. Here B^+ is the ionic rotational constant and N^+ signifies the end-over-end rotation. Higher order rotational contributions were left out because their effect is small compared to the resolution of the magnetic bottle spectrometer (8–10 meV). The calculated spectrum is convoluted with a full width at half maximum of 18 meV. Our measurements indicate that in this wavelength region ionization only takes place to the $X\,^2\Sigma_g^+(v^+=0)$ ionic state. No transitions to higher vibrational levels or transitions to other ionic states were observed. Photoelectron spectra of N_2 produced in its first vibrational level are also measured. These spectra show similar behavior as observed for the (0,0) $Q(72)$ rotational transition shown in Fig. 3, with one dominant peak (ΔN

$=0$) and smaller $\Delta N=\pm 2$ peaks on either side. Ionization of N_2 *via* $a''\,{}^1\Sigma_g^+$ $(v'=1)$ takes place to $X\,{}^2\Sigma_g^+$ $(v^+=1)$, again showing $\Delta v=0$ propensity.

Even though the calculated photoelectron spectra shown in Fig. 3(b) are for $N'=72$, the spectra originating from other N' in this experiment are similar since at these high N levels, contributions from the 3-*j* symbols in Eq. (2) do not play an important role, i.e., they have reached the high N limit. In the calculated spectra, the $\Delta N=\pm 2$ peaks show almost equal intensity due to the high N value and the small difference in photoelectron kinetic energy. As can be seen in Figs. 3(a) and 3(b) the agreement between measured and calculated spectra is excellent. Both spectra show the same important features, *viz*. a dominant peak resulting from the $\Delta N=0$ transition, two small peaks from the $\Delta N=\pm 2$ transitions, and no peaks from the $\Delta N=\pm 1,\pm 3$ transitions. Virtually zero intensity was calculated for the $\Delta N=\pm 4$ transitions, in agreement with the fact that these transitions are not visible in the measured photoelectron spectra. The spectra were calculated assuming alignment appropriate to a two-photon excitation as well as for an isotropic population of M_J levels. These two resulting spectra were very similar and indistinguishable on the scale of our figures. Furthermore, since the optical transition responsible for the dissociation of N_2O is parallel (about 97%, Ref. 5), the N_2 molecule is expected to begin rotating in a plane containing the polarization of the laser, and one would expect the population in the $M_J=0$ level to be dominant. To explore this effect we also calculated the spectra assuming only the $M_J=0$ level to be populated. The $\Delta N=2/\Delta N=-2$ peaks were somewhat larger, 0.348/0.353, with this assumption $(M_J=0)$ than for the case of two-photon induced alignment, 0.208/0.213 relative to a $\Delta N=0$ peak intensity of 1. The fact that the experimentally observed intensity for the $\Delta N=\pm 2$ peaks is smaller than the value calculated assuming complete alignment in $M_J=0$ cannot originate from a loss of such alignment by a single collision in the time between dissociation of N_2O and detection of N_2. This time is maximally the 20 ns duration of the laser pulse and with the number density at 1 mTorr in the crossing region this would imply a vanishing collision probability $(\sim 10^{-6})$ for a typical gas collision cross section. Whatever its cause, it seems that this expected strong alignment in $M_J=0$ of the N_2 molecule does not manifest itself in these experiments as agreement with spectra calculated assuming isotropic distribution appears better.

As we have mentioned earlier, based on the atomic model, we would predict rather weak $\Delta N=\pm 2$ and ± 4 intensities for a photoelectron carrying mostly the *p* wave. Indeed, this is the case for both measured and calculated spectra, suggesting that the underlying photoelectron dynamics should be very atomic-like. Close examination of the photoelectron matrix elements, however, reveals that the photoionization shows significant molecular character. Figure 4 shows the magnitude $|D_l^{(-)}|$ of the [incoming-wave normalized, see Eq. (6)] partial wave components of the photoelectron matrix elements as a function of photoelectron kinetic energy for the $k\sigma_u$ channel (a) and $k\pi_u$ channel (b). $|D_l^{(-)}|$ is defined as $|\tilde{I}_{l00}|$ for the $k\sigma_u$ channel and $|\tilde{I}_{l11}|$ for the $k\pi_u$ channel where $\tilde{I}_{l\lambda\mu}$ is given in Eq. (4). Note that $|D_l^{(-)}|$ is the magnitude of only one of the μ components of $\tilde{I}_{l\lambda\mu}$ of Eq. (4). One sees that at all energies the f $(l=3)$ partial wave matrix element is always larger than that of the $p(l=1)$ wave in both ionization channels. With the dominant *s* character of the $4\sigma_g$ orbital, atomic-like expectations would suggest that the *p* wave contribution should be larger than that of the *f* wave. One would further expect, on the basis of conservation of angular momenta, that an *f* wave photoelectron matrix element of this magnitude would lead to a strong intensity for $\Delta N=\pm 2$ transitions. However, we see relatively weak transitions for these peaks. This suggests that interference among partial waves in both ionization channels and the unfavorable 3-*j* symbols result in the weak intensities seen for these $\Delta N=\pm 2$ peaks. These *f* partial waves arise from the coupling of angular momenta of the photoelectron due to torques associated with the molecular ion potential.

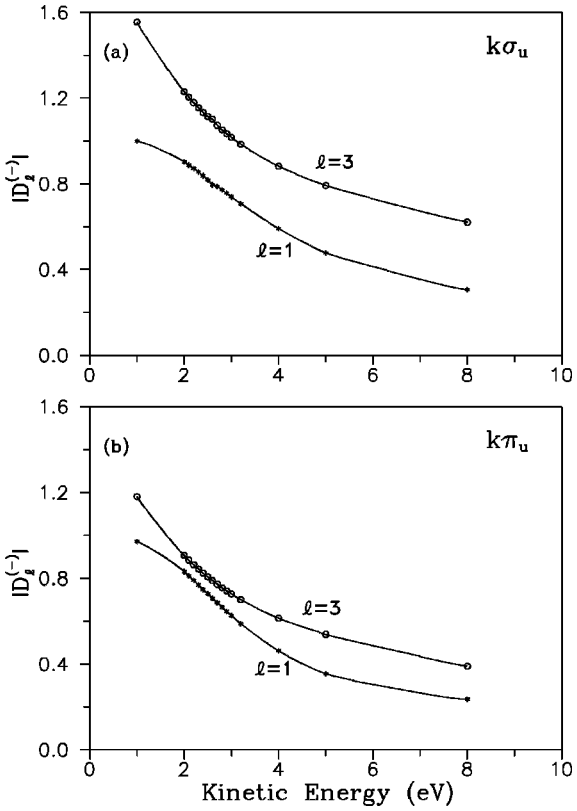

FIG. 4. Magnitude of the partial wave components of the photoelectron matrix element $|D_l^{(-)}|$ for photoionization of the $a''\,{}^1\Sigma_g^+$ resonant state of N_2 leading to the $X\,{}^2\Sigma_g^+$ state of N_2^+ *via* the $4\sigma_g \rightarrow k\sigma_u$ (a) and $4\sigma_g \rightarrow k\pi_u$ (b) ionization channels.

V. CONCLUSIONS

The photoionization dynamics of highly rotationally excited N_2 fragmented from the photodissociation of N_2O have been studied by rotationally resolved photoelectron spectroscopy. The photodissociation of N_2O via the bent $^1\Delta$ excited state results in rotationally hot N_2 photofragments, mostly in the vibrational ground level. A rotational distribution of N_2 extending from $N''=49$ up to $N''=94$ is observed and assigned for the vibrational ground level. Moreover, we were able to assign some of the peaks at the red end of the exci-

tation spectrum as arising from N_2 produced in the first vibrational level. The rotationally resolved photoionization spectra of the $a''\,^1\Sigma_g^+$ Rydberg state of N_2 leading to the $X\,^2\Sigma_g^+$ ionic state of N_2^+, were studied both experimentally and theoretically. The agreement between measured and calculated spectra is excellent.

ACKNOWLEDGMENTS

A.M.R. acknowledges the Holland Research School of Molecular Chemistry for a Ph.D. fellowship. The authors thank Ing. D. Bebelaar for technical support. Work at the California Institute of Technology was supported by a grant from the National Science Foundation (U.S.).

[1] T. E. Graedel and P. J. Crutzen, *Atmospheric Change: An Earth System Perspective* (Freeman, New York, 1992).
[2] J. T. Houghton, L. G. M. Filho, D. J. Griggs, and K. Maskell, *Stabilization of Atmospheric Greenhouse Gases: Physical, Biological and Socio-economic Implications*, World Meteorological Organization, IPCC Technical Paper III (IPCC, Geneva, Switzerland, 1997).
[3] K. F. Preston and R. F. Barr, J. Chem. Phys. **54**, 3347 (1971).
[4] D. G. Hopper, J. Chem. Phys. **80**, 4290 (1984).
[5] J. M. Teule, G. C. Groenenboom, D. W. Neyer, D. W. Chandler, and M. H. M. Janssen, Chem. Phys. Lett. **320**, 177 (2000).
[6] J. W. Rabalais, J. M. McDonald, V. Scherr, and S. P. McGlynn, Chem. Rev. **71**, 73 (1971).
[7] Th. F. Hanisco and A. C. Kummel, J. Phys. Chem. **97**, 7242 (1993).
[8] T. Suzuki, H. Katayanagi, Y. Mo, and K. Tonokura, Chem. Phys. Lett. **256**, 90 (1996).
[9] D. W. Neyer, A. J. R. Heck, and D. W. Chandler, J. Chem. Phys. **110**, 3411 (1999).
[10] D. W. Neyer, A. J. R. Heck, D. W. Chandler, J. M. Teule, and M. H. M. Janssen, J. Phys. Chem. A **103**, 10388 (1999).
[11] J. M. Teuel, Ph.D. thesis, Vrije Universiteit, Amsterdam, 1997.
[12] M. Ahmed, E. R. Wouters, D. S. Peterka, O. S. Vasyutinskii, and A. G. Suits, Faraday Discuss. **113**, 425 (1999).
[13] K. R. Lykke and B. D. Kay, J. Chem. Phys. **95**, 2252 (1991).
[14] Th. F. Hanisco and A. C. Kummel, J. Phys. Chem. **95**, 8565 (1991).
[15] Th. F. Hanisco and A. C. Kummel, J. Phys. Chem. **96**, 2982 (1992).
[16] M. H. M. Janssen, J. M. Teule, D. W. Neyer, D. W. Chandler, and G. C. Groenenboom, Faraday Discuss. **113**, 473 (1999).
[17] C. A. de Lange, in *High Resolution Laser Photoionization and Photoelectron Studies*, edited by I. Powis, T. Baer, and C. Y. Ng (Wiley, New York, 1995), p. 195.
[18] C. A. de Lange, J. Chem. Soc., Faraday Trans. **94**, 3409 (1998).
[19] C. A. de Lange, Adv. Chem. Phys. **117**, 1 (2001).
[20] R. R. Lucchese, G. Raseev, and V. McKoy, Phys. Rev. A **25**, 2572 (1982).
[21] K. Wang and V. McKoy, J. Chem. Phys. **95**, 4977 (1991).
[22] S. T. Pratt, P. M. Dehmer, and J. L. Dehmer, J. Chem. Phys. **78**, 4315 (1983).
[23] M. A. O'Halloran, S. T. Pratt, P. M. Dehmer, and J. L. Dehmer, J. Chem. Phys. **87**, 3288 (1987).
[24] S. T. Pratt, E. F. McCormack, P. M. Dehmer, and J. L. Dehmer, J. Chem. Phys. **92**, 1831 (1990).
[25] C. R. Scheper, W. J. Buma, C. A. de Lange, and W. J. van der Zande, J. Chem. Phys. **109**, 8319 (1998).
[26] S. T. Pratt, P. M. Dehmer, and J. L. Dehmer, J. Chem. Phys. **92**, 262 (1990).
[27] C. R. Scheper, M. F. Somers, and C. A. de Lange, J. Electron Spectrosc. Relat. Phenom. **108**, 123 (2000).
[28] E. de Beer, C. A. de Lange, J. A. Stephens, K. Wang, and V. McKoy, J. Chem. Phys. **95**, 714 (1991).
[29] E. de Beer, M. Born, C. A. de Lange, and N. P. C. Westwood, Chem. Phys. Lett. **186**, 40 (1991).
[30] K. Wang, J. A. Stephens, V. McKoy, E. de Beer, C. A. de Lange, and N. P. C. Westwood, J. Chem. Phys. **97**, 211 (1992).
[31] J. B. Milan, W. J. Buma, C. A. de Lange, K. Wang, and V. McKoy, J. Chem. Phys. **107**, 2782 (1997).
[32] C. A. de Lange, in *The Role of Rydberg States in Spectroscopy and Reactivity*, edited by C. Sandorfy (Kluwer Academic, Dordrecht, 1999), p. 457.
[33] T. A. Miller, T. Suzuki, and E. Hirota, J. Chem. Phys. **80**, 4671 (1984).
[34] A. M. Rijs, E. H. G. Backus, C. A. de Lange, N. P. C. Westwood, and M. H. M. Janssen, J. Electron Spectrosc. Relat. Phenom. **112**, 151 (2000).
[35] K. Wang and V. McKoy, Annu. Rev. Phys. Chem. **46**, 275 (1995).
[36] W. J. Hunt and W. A. Goddard, Chem. Phys. Lett. **3**, 414 (1969).
[37] T. H. Dunning, Jr., J. Chem. Phys. **53**, 2823 (1970); **55**, 3958 (1971).
[38] G. Selwyn, J. Podolske, and H. S. Johnston, Geophys. Res. Lett. **4**, 427 (1977).
[39] J. Xie and R. N. Zare, J. Chem. Phys. **93**, 3033 (1990).
[40] J. Bendtsen, J. Raman Spectrosc. **2**, 133 (1974).